

Robust Quantum Control via Multipath Interference for Thousandfold Phase Amplification in a Resonant Atom Interferometer

Yiping Wang*,¹ Jonah Glick*,¹ Tejas Deshpande*,¹ Kenneth DeRose*,¹ Sharika Saraf,¹ Natasha Sachdeva,^{1,2} Kefeng Jiang,¹ Zilin Chen,¹ and Tim Kovachy^{1,†}

¹*Department of Physics and Astronomy and Center for Fundamental Physics, Northwestern University*

²*Q-CTRL, Quantum Applications and Algorithms Division*

We introduce a novel technique for enhancing the robustness of light-pulse atom interferometers against the pulse infidelities that typically limit their sensitivities. The technique uses quantum optimal control to favorably harness the multipath interference of the stray trajectories produced by imperfect atom-optics operations. We apply this method to a resonant atom interferometer and achieve thousand-fold phase amplification, representing a fifty-fold improvement over the performance observed without optimized control. Moreover, we find that spurious interference can arise from the interplay of spontaneous emission and many-pulse sequences and demonstrate optimization strategies to mitigate this effect. Given the ubiquity of spontaneous emission in quantum systems, these results may be valuable for improving the performance of a diverse array of quantum sensors. We anticipate our findings will significantly benefit the performance of matter-wave interferometers for a variety of applications, including dark matter, dark energy, and gravitational wave detection.

Quantum sensing is a powerful tool for fundamental physics tests [1, 2], which include precision measurements of oscillating signals [1–20]. Resonant [21–26] light-pulse atom interferometers [19, 20, 27–35], a class of light-pulse atom interferometers [36–39], employ sequential mirror pulses to induce periodic reversals in the directions of the interferometer arms, intertwining their spacetime trajectories into loops repeating at a tunable target frequency (Fig. 1). Resonant atom interferometers have been proposed as powerful sensors of various oscillatory signals, including those from gravitational waves [14, 35, 40–42], dark matter [7–9, 14, 15, 34], dark energy [19], accelerations [8, 20, 29], and rotations [20]. Increasing the number of loops enhances interferometer sensitivity at the target frequency and suppresses off-resonant noise, akin to applying lock-in detection [43–51] and dynamical decoupling [52–57] to matter waves.

A critical challenge impeding the full metrological potential of resonant light-pulse atom interferometers is the adverse impact of mirror pulse infidelities, which limit the total number of loops that can be performed [20, 29, 33]. With imperfect pulse efficiency, each atom’s wavefunction diverges into many ‘stray’ paths that deviate from the central two interferometer arms (Fig. 1), thereby diminishing the population contributing to the signal and/or introducing deleterious effects through multipath interference [32, 58][59].

Experimental tradeoffs and imperfections inevitably result in mirror pulse infidelities. Two experimental parameters relevant to such tradeoffs are the temperature of the atom cloud and the ratio of the interferometer laser beam waist to the atom cloud size, noting that practical limitations exist on how small the atom cloud can be made [15, 60–62]. Accepting a hotter cloud can simplify and expedite cloud preparation and enable larger atom numbers, but can lead to large thermal Doppler detuning spreads which degrade pulse fidelities [15, 63].

With typical constraints on the total interferometer beam power, decreasing the beam waist increases intensity inhomogeneity across the cloud—which adversely affects pulse fidelity—but advantageously increases the peak intensity [15]. A large intensity reduces the susceptibility of the pulse efficiency to Doppler detunings [64], allows more pulses per unit time—key for the efficacy of clock atom interferometers which use single-photon transitions on narrow clock lines [11–13, 65–68], especially in parallel operation [15, 35]—and enables reduced incoherent photon scattering for multi-photon Raman, Bragg [36, 37, 69], or clock [70] atom optics. Such tradeoffs are especially pronounced for long-baseline interferometry [13–18, 71–73] and portable sensors with hotter atom clouds [38, 39]. A maximum of 400 loops has been achieved, but required preparing a Bose-Einstein condensate confined in a waveguide to attain single-pulse efficiencies of 99.4% [33]. It is therefore essential to develop resonant atom interferometers where the signal remains robust against mirror pulse infidelities, directly mitigating the drawbacks associated with experimental tradeoffs.

Traditionally, individual beamsplitter or mirror operations in light-pulse atom interferometers [74], including large momentum effective atom optics operations composed of sequences of many pulses [36], have been made robust using composite pulses [75–77], adiabatic rapid passage [29, 78, 79], Floquet pulse engineering [68] or acceleration [80], quantum optimal control (QOC) [81–89], and coherent enhancement of Bragg pulse sequences [90]. These methods usually, though not always [80, 90], require increased pulse area and/or duration, leading to increased signal degradation from incoherent photon scattering and/or reducing the number of pulses that can be applied per unit time. Moreover, despite enhancements from these methods, atom optics operations inevitably retain residual infidelities.

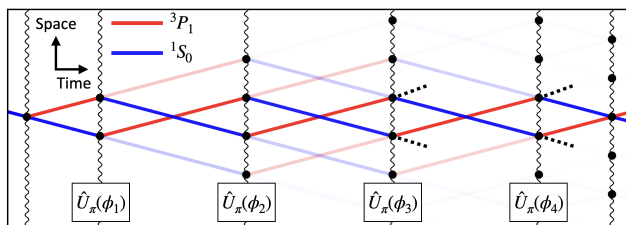


FIG. 1. Resonant light-pulse atom interferometry: Mirror (π) and beamsplitter pulses split, redirect, and interfere interferometer arms (atom-laser interactions at black dots). Imperfect mirror operations $\hat{U}_\pi(\phi_i)$ create stray paths. The laser phases for the mirror pulses (ϕ_i for the i th pulse) are control parameters tuned via quantum optimal control to limit the spatial spread of trajectories, leveraging intra-sequence interference between trajectories. Dashed black lines indicate trajectories suppressed through destructive interference. Greater opacity of the atom paths (blue and red) denotes larger population.

We instead introduce the method of making the entire interferometer sequence robust to imperfections in individual mirror operations by leveraging QOC [91–100] in a novel way to advantageously harness multipath interference between numerous stray trajectories. As a demonstration, we utilize this method to enhance the robustness of a resonant single-photon clock atom interferometer to pulse infidelities, achieving 50-fold improvement in the resonant signal amplification—for a total of more than 500 loops—in spite of an individual pulse transfer efficiency of $\approx 90\%$, representative of what one might encounter for a long-baseline atom interferometer [15] such as MAGIS-100 [13]. Moreover, we elucidate how the interplay between spontaneous emission and many-pulse sequences can generate spurious interference signals with surprisingly high visibility that obscure the signals of interest, and demonstrate an optimization approach to circumvent this effect. These findings may be valuable for improving the performance of a variety of quantum sensors which are vulnerable to the effects of spontaneous emission [101, 102]. Our general approach is not constrained by the specific type of atom optics, and we anticipate that it will enable higher levels of precision across various atom interferometer designs, including those based on multi-photon transitions.

Apparatus.— A horizontal laser beam [103] tuned to the 689 nm 1S_0 – 3P_1 ($m_j = 0$) intercombination line performs interferometry on a cloud of ^{88}Sr atoms released from a 3D magneto-optical trap. The intermediate 21.6 μs lifetime of this transition is long enough to be suitable for clock atom interferometry and enables high (MHz-scale) Rabi frequencies with Watt-scale interferometer beams [67, 68], which is advantageous for measuring up to MHz-scale signals, such as in dark matter searches [3]. After an interferometer sequence, a 461 nm push beam spatially separates the ground state from the ex-

cited state; then the two populations are read out via fluorescence detection [67, 68]. The interferometer fringe visibility (v) and phase ($\Delta\phi$) are extracted by fitting the normalized excited state population (P_e) as a function of the final beamsplitter phase (ϕ_b), to the expression $\frac{1}{2}(1 + v \cos[\Delta\phi + \phi_b])$. An M-Labs ARTIQ timing system controls the power, phase, and duration of each pulse via an acousto-optic modulator. The ratio of the laser beam waist to the atom cloud size (≈ 3) and the ratio of the Doppler detuning spread to Rabi frequency (≈ 0.1) used in this work [104] are representative of the ratios anticipated for MAGIS-100.

Open-loop optimization with QOC. We use a semi-classical model [105–107] to compute the spread of trajectories in a multi-loop interferometer under imperfect mirror operations for a particular choice of laser phases [104]. We apply QOC to these interferometers by selecting the laser phases of the mirror pulses as control parameters [53, 82] and defining a cost function aimed at minimizing the spatial spread of trajectories throughout the interferometer cycle [104]. Our approach leverages the fact that stray trajectories spawned by one π -pulse can spatially overlap and interfere with those spawned by previous π -pulses. The phase of the laser is imprinted on kicked trajectories, which we find can facilitate destructive interference among paths diverging from the central interferometer arms and constructive interference among stray paths that rejoin them, as visualized in Fig 2 (a-b).

We define an N -dimensional optimization problem where the phases of the first N mirror pulses repeat L/N times to compose an L -loop interferometer. We arrive at the sequence characterized in Figures 2 and 3 by tuning the phases of the mirror pulses to minimize the spread of trajectories over a set of $N = 8$ laser phases repeated 8 times. Our optimization approach not only yields sequences that prove effective experimentally, but also provides a visual explanation of why certain sequences outperform others. For example, we notice that for the case of $L = 8$, the universally robust (UR) UR-8 dynamical decoupling sequence, originally derived under an entirely different framework [57], provides near-optimal results per our cost function. Following the metrics used in [57] would suggest that for L loops, it is best to implement the corresponding UR- L sequence. For larger L , however, we observe that applying UR- L to a resonant atom interferometer leads to a reduced interferometer phase sensitivity to resonantly oscillating signals. The semi-classical model visually illustrates the reason for this: The further a trajectory strays from the central arms, the less phase information it carries about the resonantly oscillating signal due to the fewer imprinted laser phases. The UR- L sequence leads to a spread of spatial trajectories which increases with L , thereby reducing overall interferometer sensitivity to oscillating signals as L increases. Applying the spatial spread cost optimization for $N = 8$ at large L produces pulse phases which happen to coincide with

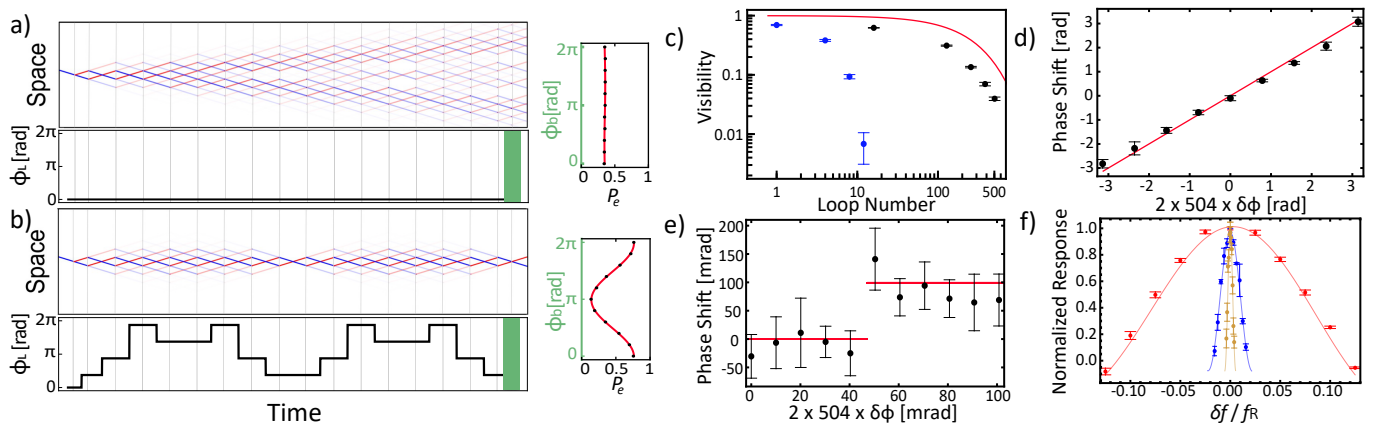


FIG. 2. Introduction to the $N=8$ -pulse sequence with optimized phases ($\frac{3\pi}{8}, \frac{7\pi}{8}, \frac{15\pi}{8}, \frac{11\pi}{8}, \frac{11\pi}{8}, \frac{15\pi}{8}, \frac{7\pi}{8}, \frac{3\pi}{8}$). A comparison of the spatial spread of trajectories, the laser phases ϕ_L , and experimentally collected interferometer fringes in 16-loop unoptimized (a) and optimized (b) sequences. (c) Interferometer fringe visibility as a function of loop number for optimized (black) and unoptimized (blue) sequences. The red curve indicates the spontaneous emission limit. Error bars are generated via standard error from fits of the interferometer fringes. (d) The phase amplification of the optimized sequence observed after 504 loops. Each data point represents an average derived from five fringe scans, with error bars calculated from the standard deviation. (e) Leveraging the enhanced interferometer phase sensitivity to resolve the bit discretization of the phase control system in a 504 loop interferometer sequence. Red horizontal lines indicate expected phase shifts due to discretization effects. Average values and error bars, generated from standard error of the mean, are evaluated from nine fringe scans. (f) Data of the self-normalized resonant response vs. offset (δf) from resonant frequency (f_R) with theory curves for the optimized sequence for loop numbers 8 (red), 64 (blue), and 256 (yellow). Error bars are generated via standard error from fits of the interferometer fringes.

a repeated UR-8 pattern—outperforming UR- L in our application—and optimizing over $N = 16$ phases produces sequences distinct from the UR- N formula owing to the reduced phase sensitivity associated with the UR- N sequences at high N . Extending our optimization from $N = 8$ to $N = 16$ enhances the interferometer visibility by 1.5x in a 496-loop interferometer, while maintaining sensitivity to oscillating signals [104]. The cost function can be tuned to adjust how strongly the population in stray trajectories is penalized as a function of distance from the central arms. Limiting the spread of trajectories could be useful for accommodating constraints on the interferometer size, like in cases where the interferometer needs to fit inside a satellite [35] or a magnetically shielded region [9].

The $N = 8$ optimized sequence enables a 50x increase in the loop number. Fig. 2(c) demonstrates that with optimized laser phases, interferometer visibility degrades more gradually than in the unoptimized case as loop number increases. Consequently, interferometer visibility can be resolved beyond 500 loops compared to the maximum 10 loops for the unoptimized sequence under the same imperfect atom-optics pulses. The red curve is a fundamental visibility limit set by the $21.6 \mu\text{s}$ lifetime of the 3P_1 state—our data is within a factor of 4 of this limit [104]. We use 80 ns π pulse durations, with 80 ns of dead-time between pulses. Further, by increasing the dead-time, we experimentally verify that the benefits of the optimization are preserved when the distance between neighboring atom-laser interactions points (where differ-

ent sets of trajectories converge (Fig. 1)) is increased beyond a coherence length; we only observe a reduction in visibility consistent with the effects of spontaneous emission as the interferometer duration is increased [104].

We demonstrate that the phase response of the interferometer with the optimized sequence and imperfect mirror pulses is comparably sensitive to resonantly oscillating signals as the expected response of an interferometer with perfect atom-optics pulses at $L = 504$ loops. We apply a signal in the form of an oscillating laser phase, $\delta\phi \sin(\omega t_i)$, added to i th mirror pulse of the optimized sequence, where the pulse occurs at time t_i . An analogous signal could emerge from motion of the atom relative to the laser beam, which results in a change in phase associated with each atom-light interaction [104]. Moreover, when transforming into a frame that rotates with the oscillating laser phase, the dynamics of the system are equivalent to one in which there are oscillations in the atom’s resonance frequency [64], e.g. due to dark matter [7]. In Fig. 2(d), the interferometer phase response to a resonantly oscillating signal is in close agreement with the expected signal amplification factor of $2L \approx 1000$, indicated by the red line. In Fig. 2(e), we leverage this thousandfold amplification to resolve the digitization inherent to the AD9910 Direct Digital Synthesizer used to modulate the interferometer beam’s phase. The 16 bit phase resolution introduces observable discrete jumps of $\frac{2\pi}{2^{16}} = 96 \mu\text{rad}$, attributed to the toggling of the least significant bit. Fig. 2(f) shows the narrowing of the resonant response as a function of signal frequency as

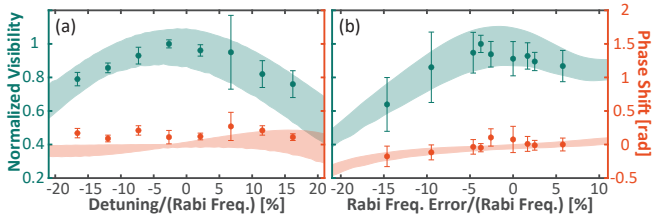


FIG. 3. Susceptibility of the $N = 8$ optimized sequence to detuning (a) and Rabi frequency error (b) at 504 loops, as determined by experiment (solid dots), and simulation (shaded bands, width indicating uncertainty). The interferometer visibilities (blue) are normalized to their maximum value, and the interferometer phase is displayed in red. Each data point is the average obtained from 5 individual fringe scans with the error bar being the standard deviation. The detuning is plotted relative to the estimated Rabi frequency for atoms at the center of the cloud [104].

loop number is increased, consistent with the theoretical response function of an interferometer with perfect atom-optics operations [104].

In Fig. 3, we examine the resilience of the optimized sequence to deviations in overall laser detuning and Rabi frequency by deliberately introducing errors in these parameters on the order of 10% of the nominal Rabi frequency. Despite these variations, the interferometer phase remains robust within approximately ± 100 mrad and the visibility remains above 50% of its peak value.

Spurious interference from spontaneous emission. Spontaneous emission occurs stochastically throughout the interferometer sequence [108], causing atoms to lose all prior phase information stored between the ground and excited states upon decay. Spontaneous emission is commonly treated as contributing to an incoherent background in atom interferometry [109]. However, atoms undergoing spontaneous emission during a pulse can re-emerge into a coherent superposition due to the remaining pulse duration, with the phase of the laser imprinted onto the phase of the transferred population. We find that certain repeating phase sequences can synchronize the re-emerging atomic coherence from one pulse with that from previous pulses, leading to the build-up of an interference signal with a well-defined cumulative phase that is largely insensitive to oscillating signals of interest. At high loop numbers, this spurious interference pattern sometimes becomes dominant, obscuring the intended signal (Fig.4). Furthermore, we find that imposing specific constraints on the pulse sequence can suppress this spurious interference by making the final phase distribution of the decayed atoms average to zero—for example, groups of $N = 8$ mirror pulses with the pattern $\phi_1, \phi_2, \phi_2 + \pi, \phi_1 + \pi, \phi_1 + \pi, \phi_2 + \pi, \phi_2, \phi_1$ for arbitrary phases ϕ_1 and ϕ_2 . We note that the open-loop optimized sequence obeys this constraint. Fig. 4 depicts both a phase sequence that leads to cumulative phase buildup

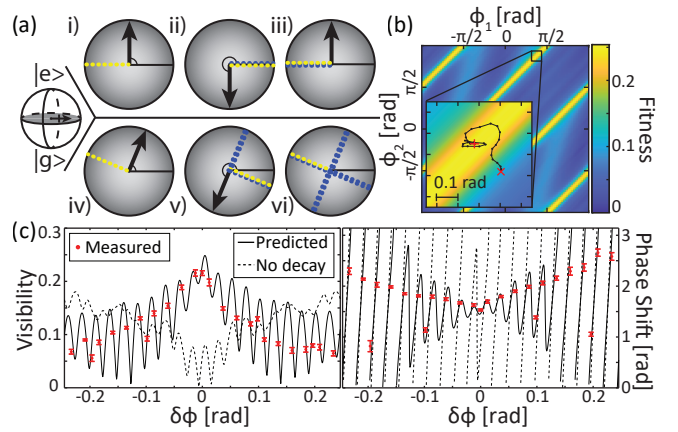


FIG. 4. (a) Simplified depiction of a Bloch sphere from a top-down view, composed of only atoms that have undergone spontaneous emission decay. The black arrow indicates the axis of state rotation based on the pulse phase, the yellow represents the semicircular arc formed due to atom decay at various times during the corresponding pulse and subsequent state rotation during the remainder of the pulse, and the blue represents arcs from previous pulses. (i,ii,iii) Bloch sphere after the first, second, and third mirror pulses, respectively, in the alternating $\pm\pi/2$ phase sequence, showing a non-zero phase formed cumulatively from decayed atoms. (iv,v,vi) Bloch sphere after the first, fourth, and eighth mirror pulses, respectively, in the optimized phase sequence (see Fig. 2), which achieves a symmetric distribution of decayed atoms (arrow removed for visual clarity in vi). (b) Simulation results of fitness values for pulse sequences over the ϕ_1 - ϕ_2 parameter space (see main text). The inset details an example optimization trajectory for the closed-loop search method (“x”: starting point, “+”: open-loop optimization result). (c) Visibility and phase shift for the alternating $\pm\pi/2$ phase sequence over 128 loops vs. amplitude $\delta\phi$ of a resonantly oscillating signal. For $|\delta\phi| \lesssim 0.1$, visibility markedly increases, but the phase shift shows a largely insensitive response. For example, when shifting from $\delta\phi = 0$ to the neighboring data point with $\delta\phi = \pi/256$, the phase shift for a fully phase sensitive sequence—such as our optimized sequence—would change by approximately π . Here, the phase shift only changes by $\mathcal{O}(100$ mrad). Data are consistent with simulations that include spontaneous emission decay (solid curves) and diverge from those excluding it (dashed curves).

involving mirror pulses with phase alternating between $\pm\pi/2$ [110], and another where we have successfully mitigated this effect using the above constraint. To conceptually illustrate cumulative phase build-up, we consider the interferometer in momentum space so that we can interpret our measurement as an average over atoms with a distribution of momenta p , with each atom acting as a two-level system corresponding to the coupling of states $|^1S_0, p\rangle$ and $|^3P_1, p + \hbar k\rangle$. This allows a Bloch sphere [64] visualization and optical Bloch equation (OBE) simulations [104].

Closed-loop optimization. In order to address experimental errors beyond effects captured by simulations, we

survey the ϕ_1 - ϕ_2 parameter space under the constraint described above by implementing closed-loop optimization, where optimization steps are determined by real-time experimental data [111–115]. We maximize a fitness function defined as $f = v \cos^4(\Delta\phi_0/2)$, where v is the measured visibility and $\Delta\phi_0$ is the measured phase shift without an applied signal [104]. We begin the optimization near a point that our OBE simulations suggests maximizes the fitness function. The optimization trajectory converges to a pulse sequence consistent with simulation results and with the results of the open-loop optimization (Fig. 4(b)).

Outlook. In future work, we aim to extend our optimization approach to interferometers using various types of atom optics and geometries, including those employing broadband dynamical decoupling [116] or multiloop configurations with increased momentum splittings, which in some cases can enhance sensitivity [35]. We have already experimentally demonstrated the adaptability of our open-loop optimization to improve robustness in the latter case, which will be discussed in a future manuscript.

Acknowledgements. We thank Andre Carvalho, Garrett Louie, and Viktor Perunicic for valuable discussions, and Garrett Louie also for contributions to the apparatus. This material is based upon work supported by the U.S. Department of Energy, Office of Science, National Quantum Information Science Research Centers, Superconducting Quantum Materials and Systems Center (SQMS) under contract number DE-AC02-07CH11359. This work is funded in part by the Gordon and Betty Moore Foundation (Grant GBMF7945), the David and Lucile Packard Foundation (Fellowship for Science and Engineering), the Office of Naval Research (Grant Number N00014-19-1-2181), and the National Institute of Standards and Technology (Grant Number 60NANB19D168). This research was also supported in part through the computational resources and staff contributions provided for the Quest high performance computing facility at Northwestern University which is jointly supported by the Office of the Provost, the Office for Research, and Northwestern University Information Technology. JG acknowledges support from a National Science Foundation (NSF) Quantum Information Science and Engineering Network (QISE-NET) Graduate Fellowship, funded by NSF award No. DMR-1747426.

Author Contributions. The author list is grouped into authors who led one or more areas of work (names marked by a *), followed by additional authors, followed by the principal investigator at the end. Authors within each group are listed in reverse alphabetical order. TD led apparatus design and construction. KD, JG, KJ, SS, and YW contributed equally to data collection and analysis. KD and YW led development of the closed-loop optimization approach and spontaneous emission simulations and studies, the latter with supporting contribu-

tions from JG. JG (lead), ZC (supporting), KJ (supporting), and SS (supporting) developed the open-loop optimization approach. KD (equal), NS (equal), YW (equal), JG (supporting), KJ (supporting), and SS (supporting) commissioned the cold atom source and atom interferometer. TK (lead) and TD (supporting) supervised the work. All authors contributed to conceptualization of the work and validation of the results. KD (equal), JG (equal), KJ (equal), TK (equal), SS (equal), YW (equal), ZC (supporting), TD (supporting), and NS (supporting) prepared and reviewed the manuscript.

[†] timothy.kovachy@northwestern.edu

- [1] A. Chou, K. Irwin, R. H. Maruyama, O. K. Baker, C. Bartram, K. K. Berggren, G. Cancelo, D. Carney, C. L. Chang, H.-M. Cho, *et al.*, Quantum sensors for high energy physics, arXiv preprint arXiv:2311.01930 (2023).
- [2] M. S. Safronova, D. Budker, D. DeMille, D. F. J. Kimball, A. Derevianko, and C. W. Clark, Search for new physics with atoms and molecules, *Rev. Mod. Phys.* **90**, 025008 (2018).
- [3] D. Antypas, A. Banerjee, C. Bartram, M. Baryakhtar, J. Betz, J. Bollinger, C. Boutan, D. Bowering, D. Budker, D. Carney, *et al.*, New horizons: scalar and vector ultralight dark matter, arXiv preprint arXiv:2203.14915 (2022).
- [4] S. Dimopoulos, P. W. Graham, J. M. Hogan, M. A. Kasevich, and S. Rajendran, Atomic gravitational wave interferometric sensor, *Phys. Rev. D* **78**, 122002 (2008).
- [5] L. Hollberg, E. Cornell, and A. Abdelrahmann, Optical atomic phase reference and timing, *Philosophical Transactions of the Royal Society A: Mathematical, Physical and Engineering Sciences* **375**, 20160241 (2017).
- [6] A. Banerjee, G. Perez, M. Safronova, I. Savoray, and A. Shalit, The phenomenology of quadratically coupled ultra light dark matter, *Journal of High Energy Physics* **2023**, 1 (2023).
- [7] A. Arvanitaki, P. W. Graham, J. M. Hogan, S. Rajendran, and K. Van Tilburg, Search for light scalar dark matter with atomic gravitational wave detectors, *Phys. Rev. D* **97**, 075020 (2018).
- [8] P. W. Graham, D. E. Kaplan, J. Mardon, S. Rajendran, and W. A. Terrano, Dark matter direct detection with accelerometers, *Phys. Rev. D* **93**, 075029 (2016).
- [9] P. W. Graham, D. E. Kaplan, J. Mardon, S. Rajendran, W. A. Terrano, L. Trahms, and T. Wilkason, Spin precession experiments for light axionic dark matter, *Phys. Rev. D* **97**, 055006 (2018).
- [10] L. Badurina, D. Blas, and C. McCabe, Refined ultralight scalar dark matter searches with compact atom gradiometers, *Physical Review D* **105**, 023006 (2022).
- [11] N. Yu and M. Tinto, Gravitational wave detection with single-laser atom interferometers, *General Relativity and Gravitation* **43**, 1943 (2011).
- [12] P. W. Graham, J. M. Hogan, M. A. Kasevich, and S. Rajendran, New method for gravitational wave detection with atomic sensors, *Phys. Rev. Lett.* **110**, 171102 (2013).

- [13] M. Abe, P. Adamson, M. Borcean, D. Bortoletto, K. Bridges, S. P. Carman, S. Chattopadhyay, J. Coleman, N. M. Curfman, K. DeRose, *et al.*, Matter-wave atomic gradiometer interferometric sensor (MAGIS-100), *Quantum Sci. Technol.* **6**, 044003 (2021).
- [14] Y. A. El-Neaj, C. Alpigiani, S. Amairi-Pyka, H. Araújo, A. Balaž, A. Bassi, L. Bathe-Peters, B. Battelier, A. Belić, E. Bentine, J. Bernabeu, A. Bertoldi, R. Bingham, *et al.*, AEDGE: Atomic Experiment for Dark Matter and Gravity Exploration in Space, *EPJ Quantum Technol.* **7**, 6 (2020).
- [15] S. Abend, B. Allard, I. Alonso, J. Antoniadis, H. Araújo, G. Arduini, A. S. Arnold, T. Asano, N. Augst, L. Badurina, *et al.*, Terrestrial very-long-baseline atom interferometry: Workshop summary, *AVS Quantum Science* **6**, 024701 (2024).
- [16] M.-S. Zhan, J. Wang, W.-T. Ni, D.-F. Gao, G. Wang, L.-X. He, R.-B. Li, L. Zhou, X. Chen, J.-Q. Zhong, B. Tang, Z.-W. Yao, L. Zhu, Z.-Y. Xiong, S.-B. Lu, G.-H. Yu, Q.-F. Cheng, M. Liu, Y.-R. Liang, P. Xu, X.-D. He, M. Ke, Z. Tan, and J. Luo, ZAIGA: Zhaoshan long-baseline atom interferometer gravitation antenna, *Int. J. Mod. Phys. D* **29**, 1940005 (2020).
- [17] L. Badurina, E. Bentine, D. Blas, K. Bongs, D. Bortoletto, T. Bowcock, K. Bridges, W. Bowden, O. Buchmueller, C. Burrage, *et al.*, AION: an atom interferometer observatory and network, *Journal of Cosmology and Astroparticle Physics* **2020** (05), 011.
- [18] B. Canuel, A. Bertoldi, L. Amand, E. Pozzo di Borgo, T. Chantrait, C. Danquigny, M. Dovale Álvarez, B. Fang, A. Freise, R. Geiger, *et al.*, Exploring gravity with the miga large scale atom interferometer, *Sci. Rep.* **8**, 1 (2018).
- [19] S.-w. Chiow and N. Yu, Multiloop atom interferometer measurements of chameleon dark energy in microgravity, *Physical Review D* **97**, 044043 (2018).
- [20] J. Coslovsky, G. Afek, and N. Davidson, Ac atom interferometry with quantum lock-in sensing, in *Slow Light, Fast Light, and Opto-Atomic Precision Metrology X*, Vol. 10119 (SPIE, 2017) p. 1011903.
- [21] R. P. Kafle, D. Z. Anderson, and A. A. Zozulya, Analysis of a free oscillation atom interferometer, *Physical Review A* **84**, 033639 (2011).
- [22] J. S. Pedernales, G. W. Morley, and M. B. Plenio, Motional dynamical decoupling for interferometry with macroscopic particles, *Physical review letters* **125**, 023602 (2020).
- [23] M. Horikoshi and K. Nakagawa, Suppression of dephasing due to a trapping potential and atom-atom interactions in a trapped-condensate interferometer, *Phys. Rev. Lett.* **99**, 180401 (2007).
- [24] J. Burke, B. Deissler, K. Hughes, and C. Sackett, Confinement effects in a guided-wave atom interferometer with millimeter-scale arm separation, *Physical Review A* **78**, 023619 (2008).
- [25] S. Moukouri, Y. Japha, M. Keil, T. David, D. Groswasser, M. Givon, and R. Folman, Multi-pass guided atomic sagnac interferometer for high-performance rotation sensing, *arXiv preprint arXiv:2107.03446* (2021).
- [26] D. A. Pushin, M. Arif, and D. G. Cory, Decoherence-free neutron interferometry, *Physical Review A* **79**, 053635 (2009).
- [27] B. Dubetsky and M. Kasevich, Atom interferometer as a selective sensor of rotation or gravity, *Physical Review A* **74**, 023615 (2006).
- [28] C. Schubert, S. Abend, M. Gersemann, M. Gebbe, D. Schlippert, P. Berg, and E. M. Rasel, Multi-loop atomic sagnac interferometry, *Scientific Reports* **11**, 16121 (2021).
- [29] M. Jaffe, V. Xu, P. Haslinger, H. Müller, and P. Hamilton, Efficient adiabatic spin-dependent kicks in an atom interferometer, *Physical Review Letters* **121**, 040402 (2018).
- [30] K.-P. Marzlin and J. Audretsch, State independence in atom interferometry and insensitivity to acceleration and rotation, *Physical Review A* **53**, 312 (1996).
- [31] J. M. McGuirk, G. Foster, J. Fixler, M. Snadden, and M. Kasevich, Sensitive absolute-gravity gradiometry using atom interferometry, *Physical Review A* **65**, 033608 (2002).
- [32] L. Sidorenkov, R. Gautier, M. Altorio, R. Geiger, and A. Landragin, Tailoring multiloop atom interferometers with adjustable momentum transfer, *Physical Review Letters* **125**, 213201 (2020).
- [33] H. Kim, K. Krzyzanowska, K. Henderson, C. Ryu, E. Timmermans, and M. Boshier, One second interrogation time in a 200 round-trip waveguide atom interferometer, *arXiv preprint arXiv:2201.11888* (2022).
- [34] F. Di Pumpo, A. Friedrich, and E. Giese, Optimal baseline exploitation in vertical dark-matter detectors based on atom interferometry, *AVS Quantum Science* **6** (2024).
- [35] P. W. Graham, J. M. Hogan, M. A. Kasevich, and S. Rajendran, Resonant mode for gravitational wave detectors based on atom interferometry, *Phys. Rev. D* **94**, 104022 (2016).
- [36] G. Tino and M. Kasevich, *Atom Interferometry*, EBL-Schweitzer (IOS Press, 2014).
- [37] A. D. Cronin, J. Schmiedmayer, and D. E. Pritchard, Optics and interferometry with atoms and molecules, *Reviews of Modern Physics* **81**, 1051 (2009).
- [38] K. Bongs, M. Holynski, J. Vovrosh, P. Bouyer, G. Condon, E. Rasel, C. Schubert, W. P. Schleich, and A. Roura, Taking atom interferometric quantum sensors from the laboratory to real-world applications, *Nat. Rev. Phys.* **1**, 731 (2019).
- [39] F. A. Narducci, A. T. Black, and J. H. Burke, Advances toward fieldable atom interferometers, *Advances in Physics: X* **7**, 1946426 (2022).
- [40] A. Torres-Orjuela, Detecting intermediate-mass black hole binaries with atom interferometer observatories: Using the resonant mode for the merger phase, *AVS Quantum Science* **5** (2023).
- [41] S. Baum, Z. Bogorad, and P. W. Graham, Gravitational wave measurement in the mid-band with atom interferometers, *Journal of Cosmology and Astroparticle Physics* **2024** (05), 027.
- [42] C. Schubert, D. Schlippert, S. Abend, E. Giese, A. Roura, W. Schleich, W. Ertmer, and E. Rasel, Scalable, symmetric atom interferometer for infrasound gravitational wave detection, *arXiv preprint arXiv:1909.01951* (2019).
- [43] S. Kotler, N. Akerman, Y. Glickman, A. Keselman, and R. Ozeri, Single-ion quantum lock-in amplifier, *Nature* **473**, 61 (2011).
- [44] J. M. Boss, K. Cujia, J. Zopes, and C. L. Degen, Quan-

- tum sensing with arbitrary frequency resolution, *Science* **356**, 837 (2017).
- [45] J. R. Maze, P. L. Stanwix, J. S. Hodges, S. Hong, J. M. Taylor, P. Cappellaro, L. Jiang, M. G. Dutt, E. Togan, A. Zibrov, *et al.*, Nanoscale magnetic sensing with an individual electronic spin in diamond, *Nature* **455**, 644 (2008).
- [46] G. de Lange, D. Ristè, V. Dobrovitski, and R. Hanson, Single-spin magnetometry with multipulse sensing sequences, *Physical review letters* **106**, 080802 (2011).
- [47] R. Shaniv and R. Ozeri, Quantum lock-in force sensing using optical clock doppler velocimetry, *Nature communications* **8**, 14157 (2017).
- [48] S. Schmitt, T. Gefen, F. M. Stürner, T. Uden, G. Wolff, C. Müller, J. Scheuer, B. Naydenov, M. Markham, S. Pezzagna, *et al.*, Submillihertz magnetic spectroscopy performed with a nanoscale quantum sensor, *Science* **356**, 832 (2017).
- [49] K. Shibata, N. Sekiguchi, and T. Hirano, Quantum lock-in detection of a vector light shift, *Physical Review A* **103**, 043335 (2021).
- [50] M. Zhuang, J. Huang, and C. Lee, Many-body quantum lock-in amplifier, *PRX Quantum* **2**, 040317 (2021).
- [51] S. Kolkowitz, A. C. Bleszynski Jayich, Q. P. Unterreithmeier, S. D. Bennett, P. Rabl, J. Harris, and M. D. Lukin, Coherent sensing of a mechanical resonator with a single-spin qubit, *Science* **335**, 1603 (2012).
- [52] L. Viola, E. Knill, and S. Lloyd, Dynamical decoupling of open quantum systems, *Physical Review Letters* **82**, 2417 (1999).
- [53] T. Gullion, D. B. Baker, and M. S. Conradi, New, compensated carr-purcell sequences, *Journal of Magnetic Resonance* (1969) **89**, 479 (1990).
- [54] W. Yang, Z.-Y. Wang, and R.-B. Liu, Preserving qubit coherence by dynamical decoupling, *Frontiers of Physics in China* **6**, 2 (2011).
- [55] D. A. Lidar, Review of decoherence-free subspaces, noiseless subsystems, and dynamical decoupling, *Quantum information and computation for chemistry* , 295 (2014).
- [56] M. J. Biercuk, H. Uys, A. P. VanDevender, N. Shiga, W. M. Itano, and J. J. Bollinger, Optimized dynamical decoupling in a model quantum memory, *Nature* **458**, 996 (2009).
- [57] G. T. Genov, D. Schraft, N. V. Vitanov, and T. Halfmann, Arbitrarily accurate pulse sequences for robust dynamical decoupling, *Physical Review Letters* **118** (2017).
- [58] J. Stockton, K. Takase, and M. Kasevich, Absolute geodetic rotation measurement using atom interferometry, *Physical review letters* **107**, 133001 (2011).
- [59] Note that in certain scenarios, multipath interference [117–119] has been used to destructively reduce losses in other types of atom interferometers [90, 120].
- [60] S. Loriani, D. Schlippert, C. Schubert, S. Abend, H. Ahlers, W. Ertmer, J. Rudolph, J. Hogan, M. Kasevich, E. Rasel, *et al.*, Atomic source selection in space-borne gravitational wave detection, *New Journal of Physics* **21**, 063030 (2019).
- [61] H. Ammann and N. Christensen, Delta kick cooling: A new method for cooling atoms, *Physical review letters* **78**, 2088 (1997).
- [62] S. Chu, J. Bjorkholm, A. Ashkin, J. Gordon, and L. Hollberg, Proposal for optically cooling atoms to temperatures of the order of 10⁻⁶ k, *Optics letters* **11**, 73 (1986).
- [63] H. J. McGuinness, A. V. Rakholia, and G. W. Biedermann, High data-rate atom interferometer for measuring acceleration, *Applied Physics Letters* **100** (2012).
- [64] H. J. Metcalf and P. Van der Straten, *Laser cooling and trapping* (Springer Science & Business Media, 1999).
- [65] L. Hu, N. Poli, L. Salvi, and G. M. Tino, Atom interferometry with the sr optical clock transition, *Phys. Rev. Lett.* **119**, 263601 (2017).
- [66] L. Hu, E. Wang, L. Salvi, J. N. Tinsley, G. M. Tino, and N. Poli, Sr atom interferometry with the optical clock transition as a gravimeter and a gravity gradiometer, *Classical Quantum Gravity* **37**, 014001 (2019).
- [67] J. Rudolph, T. Wilkason, M. Nantel, H. Swan, C. M. Holland, Y. Jiang, B. E. Garber, S. P. Carman, and J. M. Hogan, Large momentum transfer clock atom interferometry on the 689 nm intercombination line of strontium, *Phys. Rev. Lett.* **124**, 083604 (2020).
- [68] T. Wilkason, M. Nantel, J. Rudolph, Y. Jiang, B. E. Garber, H. Swan, S. P. Carman, M. Abe, and J. M. Hogan, Atom interferometry with floquet atom optics, *Phys. Rev. Lett.* **129**, 183202 (2022).
- [69] M. Kim, R. Notermans, C. Overstreet, J. Curti, P. Asenbaum, and M. A. Kasevich, 40 w, 780 nm laser system with compensated dual beam splitters for atom interferometry, *Optics Letters* **45**, 6555 (2020).
- [70] S. P. Carman, J. Rudolph, B. E. Garber, M. J. Van de Graaff, H. Swan, Y. Jiang, M. Nantel, M. Abe, R. L. Barclay, and J. M. Hogan, Collinear three-photon excitation of a strongly forbidden optical clock transition, arXiv preprint arXiv:2406.07902 (2024).
- [71] J. Hartwig, S. Abend, C. Schubert, D. Schlippert, H. Ahlers, K. Posso-Trujillo, N. Gaaloul, W. Ertmer, and E. M. Rasel, Testing the universality of free fall with rubidium and ytterbium in a very large baseline atom interferometer, *New J. Phys.* **17**, 035011 (2015).
- [72] P. Asenbaum, C. Overstreet, M. Kim, J. Curti, and M. A. Kasevich, Atom-interferometric test of the equivalence principle at the 10⁻¹² level, *Phys. Rev. Lett.* **125**, 191101 (2020).
- [73] C. Overstreet, P. Asenbaum, J. Curti, M. Kim, and M. A. Kasevich, Observation of a gravitational aharonov-bohm effect, *Science* **375**, 226 (2022).
- [74] An exception involves the compensation of phase errors in a three-pulse Bragg Mach-Zehnder interferometer across the beam splitter and mirror pulses [86].
- [75] D. L. Butts, K. Kotru, J. M. Kinast, A. M. Radojevic, B. P. Timmons, and R. E. Stoner, Efficient broadband raman pulses for large-area atom, *J. Opt. Soc. Am. B* , 922.
- [76] A. Dunning, R. Gregory, J. Bateman, N. Cooper, M. Himsforth, J. A. Jones, and T. Freegarde, Composite pulses for interferometry in a thermal cold atom cloud, *Phys. Rev. A* **90**, 033608 (2014).
- [77] P. Berg, S. Abend, G. Tackmann, C. Schubert, E. Giese, W. P. Schleich, F. A. Narducci, W. Ertmer, and E. M. Rasel, Composite-light-pulse technique for high-precision atom interferometry, *Phys. Rev. Lett.* **114**, 063002 (2015).
- [78] K. Kotru, D. L. Butts, J. M. Kinast, and R. E. Stoner, Large-area atom interferometry with frequency-swept raman adiabatic passage, *Phys. Rev. Lett.* **115**, 103001 (2015).

- [79] T. Kovachy, S.-w. Chiow, and M. A. Kasevich, Adiabatic-rapid-passage multiphoton bragg atom optics, *Physical Review A* **86**, 011606 (2012).
- [80] T. Rodzinka, E. Dionis, L. Calmels, S. Beldjoudi, A. Béguin, D. Guéry-Odelin, B. Allard, D. Sugny, and A. Gauguier, Optimal floquet engineering for large scale atom interferometers, arXiv preprint arXiv:2403.14337 (2024).
- [81] J. C. Saywell, I. Kuprov, D. Goodwin, M. Carey, and T. Freegarde, Optimal control of mirror pulses for cold-atom interferometry, *Phys. Rev. A* **98**, 023625 (2018).
- [82] J. Saywell, M. Carey, M. Belal, I. Kuprov, and T. Freegarde, Optimal control of raman pulse sequences for atom interferometry, *J Phys. B* **53**, 085006 (2020).
- [83] J. Saywell, M. Carey, I. Kuprov, and T. Freegarde, Biselective pulses for large-area atom interferometry, *Phys. Rev. A* **101**, 063625 (2020).
- [84] M. H. Goerz, M. A. Kasevich, and V. S. Malinovsky, Quantum optimal control for atomic fountain interferometry, in *Optical and Quantum Sensing and Precision Metrology*, Vol. 11700 (SPIE, 2021) p. 1170005.
- [85] M. H. Goerz, M. A. Kasevich, and V. S. Malinovsky, Robust optimized pulse schemes for atomic fountain interferometry, *Atoms* **11**, 36 (2023).
- [86] J. C. Saywell, M. S. Carey, P. S. Light, S. S. Szigeti, A. R. Milne, K. S. Gill, M. L. Goh, V. S. Perunicic, N. M. Wilson, C. D. Macrae, *et al.*, Enhancing the sensitivity of atom-interferometric inertial sensors using robust control, *Nature Communications* **14**, 7626 (2023).
- [87] J. Saywell, M. Carey, P. Light, S. Szigeti, A. Milne, K. Gill, M. Goh, N. Wilson, P. Everitt, N. Robins, *et al.*, Realizing software-defined quantum sensing: experimental demonstration of software-ruggedized atom interferometry for mobile quantum inertial sensing, in *Quantum Sensing, Imaging, and Precision Metrology*, Vol. 12447 (SPIE, 2023) pp. 120–129.
- [88] Z. Chen, G. Louie, Y. Wang, T. Deshpande, and T. Kovachy, Enhancing strontium clock atom interferometry using quantum optimal control, *Phys. Rev. A* **107**, 063302 (2023).
- [89] G. Louie, Z. Chen, T. Deshpande, and T. Kovachy, Robust atom optics for Bragg atom interferometry, *New Journal of Physics* **25**, 083017 (2023).
- [90] A. Béguin, T. Rodzinka, L. Calmels, B. Allard, and A. Gauguier, Atom interferometry with coherent enhancement of bragg pulse sequences, *Physical Review Letters* **131**, 143401 (2023).
- [91] J. Werschnik and E. Gross, Quantum optimal control theory, *Journal of Physics B: Atomic, Molecular and Optical Physics* **40**, R175 (2007).
- [92] N. Khaneja, T. Reiss, C. Kehlet, T. Schulte-Herbrüggen, and S. J. Glaser, Optimal control of coupled spin dynamics: design of nmr pulse sequences by gradient ascent algorithms, *J Magn. Reson.* **172**, 296 (2005).
- [93] C. P. Koch, U. Boscain, T. Calarco, G. Dirr, S. Filipp, S. J. Glaser, R. Kosloff, S. Montangero, T. Schulte-Herbrüggen, D. Sugny, *et al.*, Quantum optimal control in quantum technologies. strategic report on current status, visions and goals for research in europe, *EPJ Quantum Technol.* **9**, 19 (2022).
- [94] Q. Ansel, E. Dionis, F. Arrouas, B. Peaudecerf, S. Guérin, D. Guéry-Odelin, and D. Sugny, Introduction to theoretical and experimental aspects of quantum optimal control, arXiv preprint arXiv:2403.00532 (2024).
- [95] L. Magrini, P. Rosenzweig, C. Bach, A. Deutschmann-Olek, S. G. Hofer, S. Hong, N. Kiesel, A. Kugi, and M. Aspelmeyer, Real-time optimal quantum control of mechanical motion at room temperature, *Nature* **595**, 373 (2021).
- [96] S. Jandura and G. Pupillo, Time-optimal two- and three-qubit gates for rydberg atoms, *Quantum* **6**, 712 (2022).
- [97] J. Tian, H. Liu, Y. Liu, P. Yang, R. Betzholtz, R. S. Said, F. Jelezko, and J. Cai, Quantum optimal control using phase-modulated driving fields, *Physical Review A* **102**, 043707 (2020).
- [98] F. Poggiali, P. Cappellaro, and N. Fabbri, Optimal control for one-qubit quantum sensing, *Physical Review X* **8**, 021059 (2018).
- [99] P. Rembold, N. Oshnik, M. M. Müller, S. Montangero, T. Calarco, and E. Neu, Introduction to quantum optimal control for quantum sensing with nitrogen-vacancy centers in diamond, *AVS Quantum Science* **2** (2020).
- [100] M. M. Müller, R. S. Said, F. Jelezko, T. Calarco, and S. Montangero, One decade of quantum optimal control in the chopped random basis, *Reports on progress in physics* **85**, 076001 (2022).
- [101] M. A. Nielsen and I. L. Chuang, *Quantum computation and quantum information* (Cambridge university press, 2010).
- [102] G. S. Agarwal, Quantum statistical theories of spontaneous emission and their relation to other approaches, *Quantum Optics*, 1 (2006).
- [103] K. DeRose, T. Deshpande, Y. Wang, and T. Kovachy, High-power, low-phase-noise, frequency-agile laser system for delivering fiber-noise-canceled pulses for strontium clock atom interferometry, *Optics Letters* **48**, 3893 (2023).
- [104] See Supplemental Material, which includes Refs. [121–125], for details of the following items: the experimental setup, optimization algorithms, theoretical models and simulations of the interferometer, and the preservation of the benefits of optimization as pulse spacing is increased.
- [105] J. M. Hogan, D. M. S. Johnson, and M. A. Kasevich, Light-pulse atom interferometry (2008), arXiv:0806.3261 [physics.atom-ph].
- [106] K. Bongs, R. Launay, and M. A. Kasevich, High-order inertial phase shifts for time-domain atom interferometers, *Applied Physics B* **84**, 599 (2006).
- [107] C. Antoine and C. J. Bordé, Quantum theory of atomic clocks and gravito-inertial sensors: an update, *Journal of Optics B: Quantum and Semiclassical Optics* **5**, S199 (2003).
- [108] P. Chrostoski, S. Bisson, D. Farley, F. Narducci, and D. Soh, Error analysis in large area multi-raman pulse atom interferometry due to undesired spontaneous decay, arXiv preprint arXiv:2403.08913 (2024).
- [109] T. Kovachy, P. Asenbaum, C. Overstreet, C. Donnelly, S. Dickerson, A. Sugarbaker, J. Hogan, and M. Kasevich, Quantum superposition at the half-metre scale, *Nature* **528**, 530 (2015).
- [110] M. Bishof, X. Zhang, M. J. Martin, and J. Ye, Optical spectrum analyzer with quantum-limited noise floor, *Physical review letters* **111**, 093604 (2013).
- [111] G. Feng, F. H. Cho, H. Katiyar, J. Li, D. Lu, J. Baugh, and R. Laflamme, Gradient-based closed-loop quantum

- optimal control in a solid-state two-qubit system, *Phys. Rev. A* **98**, 052341 (2018).
- [112] S. Rosi, A. Bernard, N. Fabbri, L. Fallani, C. Fort, M. Inguscio, T. Calarco, and S. Montangero, Fast closed-loop optimal control of ultracold atoms in an optical lattice, *Physical Review A* **88**, 021601 (2013).
- [113] C. Weidner and D. Z. Anderson, Experimental demonstration of shaken-lattice interferometry, *Physical Review Letters* **120**, 263201 (2018).
- [114] L.-Y. Chih and M. Holland, Reinforcement-learning-based matter-wave interferometer in a shaken optical lattice, *Physical Review Research* **3**, 033279 (2021).
- [115] C. LeDesma, K. Mehling, J. Shao, J. D. Wilson, P. Axelrad, M. M. Nicotra, M. Holland, and D. Z. Anderson, A machine-designed optical lattice atom interferometer, *arXiv preprint arXiv:2305.17603* (2023).
- [116] M. Zaheer, N. Matjelo, D. Hume, M. Safronova, and D. Leibbrandt, Quantum metrology algorithms for dark matter searches with clocks, *arXiv preprint arXiv:2302.12956* (2023).
- [117] T. Rahman, A. Wirth-Singh, A. Ivanov, D. Gochnauer, E. Hough, and S. Gupta, Bloch oscillation phases investigated by multipath Stückelberg atom interferometry, *Physical Review Research* **6**, L022012 (2024).
- [118] L. Deng, E. W. Hagley, J. Denschlag, J. Simsarian, M. Edwards, C. W. Clark, K. Helmerson, S. Rolston, and W. D. Phillips, Temporal, matter-wave-dispersion talbot effect, *Physical Review Letters* **83**, 5407 (1999).
- [119] F. Moore, J. Robinson, C. Bharucha, B. Sundaram, and M. Raizen, Atom optics realization of the quantum δ -kicked rotor, *Physical Review Letters* **75**, 4598 (1995).
- [120] M. Robert-De-Saint-Vincent, J.-P. Brantut, C. J. Bordé, A. Aspect, T. Bourdel, and P. Bouyer, A quantum trampoline for ultra-cold atoms, *Europhysics Letters* **89**, 10002 (2010).
- [121] H.-R. Noh and W. Jhe, Analytic solutions of the optical Bloch equations, *Optics Communications* **283**, 2353 (2010).
- [122] B. T. Polyak, *Introduction to optimization* (New York, Optimization Software, 1987).
- [123] P. Asenbaum, C. Overstreet, and M. A. Kasevich, Matter waves and clocks do not observe uniform gravitational fields, *Physica Scripta* **99**, 046103 (2024).
- [124] P. I. Frazier, A tutorial on bayesian optimization (2018), *arXiv:1807.02811*.
- [125] L. P. Parazzoli, A. M. Hankin, and G. W. Biedermann, Observation of free-space single-atom matterwave interference, *Physical Review Letter* **109**, 1 (2012).